

pubs.acs.org/synthbio Letter

¹ Genetically Encoded Fluorescent Biosensor for Rapid Detection of ² Protein Expression

3 Matthew G. Eason, Antonia T. Pandelieva, Marc M. Mayer, Safwat T. Khan, Hernan G. Garcia,

4 and Roberto A. Chica*



Cite This: https://dx.doi.org/10.1021/acssynbio.0c00407



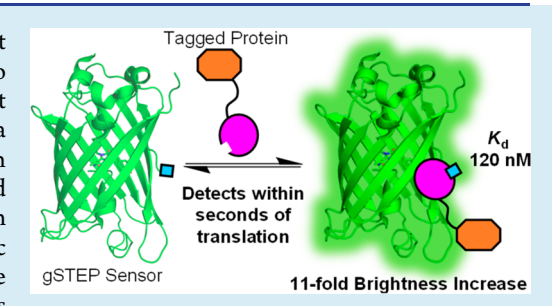
ACCESS

III Metrics & More

Article Recommendations

Supporting Information

s **ABSTRACT:** Fluorescent proteins are widely used as fusion tags to detect 6 protein expression *in vivo*. To become fluorescent, these proteins must undergo 7 chromophore maturation, a slow process with a half-time of 5 to >30 min that 8 causes delays in real-time detection of protein expression. Here, we engineer a 9 genetically encoded fluorescent biosensor to enable detection of protein 10 expression within seconds in live bacteria. This sensor for transiently expressed 11 proteins (STEP) is based on a fully matured but dim green fluorescent protein in 12 which pre-existing fluorescence increases 11-fold *in vivo* following the specific 13 and rapid binding of a protein tag ($K_{\rm d}$ 120 nM, $k_{\rm on}$ 1.7 × 10⁵ M⁻¹ s⁻¹). In live 14 *E. coli* cells, our STEP biosensor enables detection of protein expression twice as



15 fast as the use of standard fluorescent protein fusions. Our biosensor opens the door to the real-time study of short-time scale 16 processes in live cells with high spatiotemporal resolution.

17 KEYWORDS: protein engineering, green fluorescent protein, protein-peptide interaction, fluorescence

equorea victoria green fluorescent protein (GFP) and its variants are widely used as quantitative reporters of gene 20 expression to uncover the underpinnings of endogenous and 21 synthetic genetic circuits. 1-3 To become fluorescent, these 22 proteins undergo chromophore maturation, an autogenic 23 process that begins immediately following folding and involves 24 successive steps of protein backbone cyclization, dehydration, 25 and oxidation. The rate of chromophore maturation is highly 26 dependent on temperature, pH, and oxygen concentration, 27 which leads to large variations in half-times depending on 28 experimental conditions. 5 Under optimal conditions, matura-29 tion half-times for GFPs range from 5 to >30 min in E. coli. 5 30 These maturation half-times are too slow for quantitative 31 detection of fast biological processes occurring within a few 32 minutes, such as those involving transiently expressed or fast-33 degrading proteins with half-lives of less than 5 min. 6,7 As a 34 result, accurate quantification of these proteins at a given point 35 in time often requires post hoc mathematical transformations to 36 correct delays in detection of protein expression caused by 37 chromophore maturation. 8-10

To minimize the delay between translation and detection of 39 a protein of interest, biosensors that translocate a pre-40 expressed and fully matured fluorescent protein from the 41 cytosol to the nucleus following expression of a protein of 42 interest have been developed. However, the need for 43 translocation prevents these biosensors from directly detecting 44 proteins in the cytoplasm, and renders then unusable in 45 bacteria. Other biosensors use a repeating peptide fusion tag 46 on the protein of interest to recruit multiple copies of a pre-

expressed and fully matured cytosolic GFP, leading to the 47 formation of large fluorescent aggregates that can be detected 48 by fluorescence microscopy. ^{13–15} While these biosensors 49 enable real-time imaging of protein expression in individual 50 cells, their large size (>1 MDa) can interfere with the physical 51 properties of the protein of interest. Therefore, an ideal 52 biosensor for the rapid detection of protein expression *in vivo* 53 would not only minimize the delay between translation and 54 detection of the protein of interest, but would also not require 55 translocation of the fluorescent protein into a different 56 subcellular compartment, or formation of large aggregates 57 that may affect protein function.

Here, we create a genetically encoded fluorescent biosensor 59 to address these issues and enable the rapid detection of 60 protein expression within live cells. We call our sensor STEP, 61 for sensor for transiently expressed proteins (Figure 1a). 62 fl Inspired by the GCaMP family of biosensors that enable fast 63 detection of Ca^{2+} dynamics, ¹⁶ the STEP is based on a circularly 64 permuted GFP (cpGFP) that can fold and mature 65 independently of the protein of interest. In this cpGFP, the 66 N- and C-termini are located in the middle of strand β 7 of the 67 β -barrel (Figure 1b), which creates a pore on the protein 68

Received: July 30, 2020



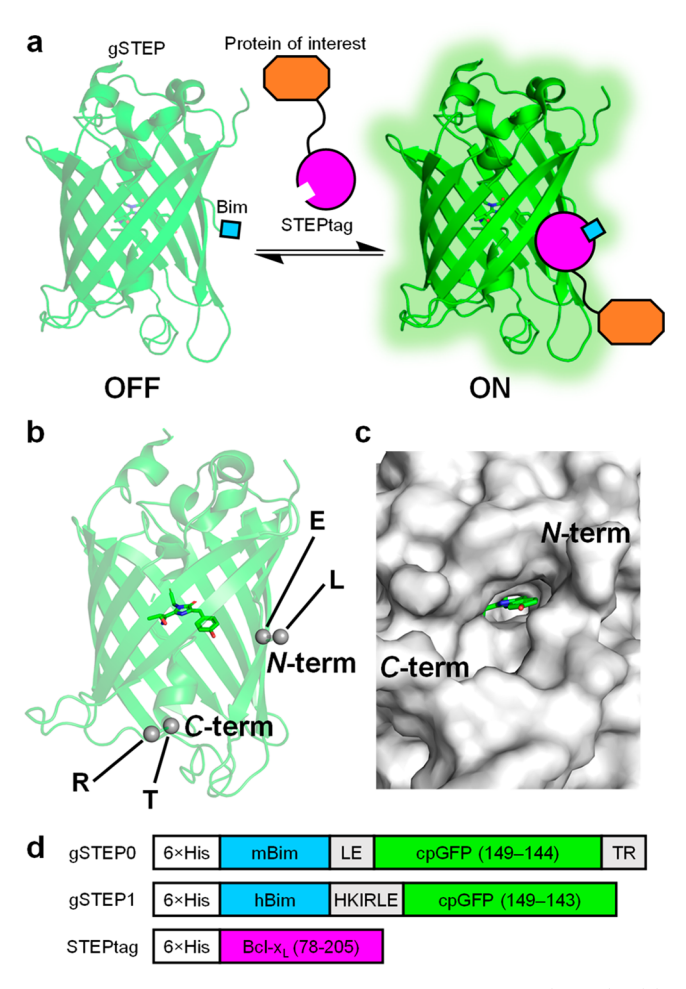


Figure 1. Sensor for transiently expressed proteins (STEP). (a) Cartoon representation of the STEP. A green fluorescent STEP (gSTEP) is expressed and allowed to mature before expression of a STEPtagged protein of interest (not to scale). Prior to STEPtag binding to the Bim peptide, gSTEP is dimly fluorescent (OFF), while the bound gSTEP emits a strong fluorescence signal (ON). (b) Crystal structure of the circularly permuted GFP from the GCaMP3 genetically encoded calcium indicator (PDB ID: 4IK8).³⁷ The chromophore is shown as sticks, and residues forming the N- and C-terminal amino acid linkers are shown as gray spheres and identified by their one-letter code. (c) Surface of the circularly permuted GFP shows a pore on the barrel surface next to the chromophore phenolate moiety (green sticks). (d) Schematic representation of gSTEP0, gSTEP1, and STEPtag. Linker sequences are shown in gray. Circularly permuted GFP (cpGFP) is shown in green, and residues are numbered according to the sequence of Aequorea victoria GFP. Bcl-x_L is shown in magenta, and residues are numbered according to the UniProt sequence (Q07817). 6× His, mBim, and hBim indicate the histidine tag, mouse Bim, and human Bim peptides, respectively.

surface directly next to the chromophore phenolate moiety 69 (Figure 1c). This pore exposes the chromophore to the 70 solvent, resulting in quenched fluorescence (Figure 1a, OFF 71 state). 17 A peptide, Bim, from the BH3 domain of the Bcl-2 72 family of eukaryotic apoptosis regulators 18 is genetically fused 73 to the N-terminus of cpGFP, creating a green fluorescent 74 STEP (gSTEP). This Bim peptide has no endogenous activity 75 in E. coli, 19 but in our system it enables specific binding of a 76 protein tag (STEPtag) derived from another Bcl-2 family 77 protein, Bcl-x_L.²⁰ Formation of the gSTEP/STEPtag complex 78 causes a change to the electrostatic environment of the 79 chromophore, restoring bright fluorescence (Figure 1a, ON 80 state). By expressing gSTEP and allowing its chromophore to 81 mature before expression of the STEPtagged protein of interest 82 is initiated, the biosensor is ready to detect its target as it is 83 expressed and folded, helping to eliminate delays in detection 84 of protein expression caused by maturation.

To create the first prototype of the sensor, gSTEP0, we 86 fused the helical mouse Bim peptide (26 amino acids) to the 87 cpGFP from the genetically encoded calcium indicator 88 GCaMP3,¹⁷ and retained the N- and C-terminal linkers on 89 either side of the barrel pore (Leu-Glu and Thr-Arg, 90 respectively), which have been shown to be important to the 91 fluorescence response of these calcium sensors (Figure 1d, 92 Supplementary Table S1). 16 The STEPtag (15.5 kDa) was 93 created by truncating the N- and C-termini of human Bcl-x₁ 94 (Figure 1d, Supplementary Table S1) to remove structural 95 elements that are not essential for binding to Bim but can 96 cause formation of a domain-swapped dimer, 21,22 and a 97 hydrophobic membrane-anchor domain, respectively. 23,24 98 Addition of a saturating concentration of purified STEPtag 99 to gSTEP0 resulted in an intensiometric fluorescence increase 100 $(\Delta F/F_0$, calculated as $(F_{\rm max}-F_{\rm min})/F_{\rm min})$ of 1.4 \pm 0.1, with a 101 dissociation constant $(K_{\rm d})$ of 250 \pm 40 nM (Supplementary 102 Figure S1, Table 1). Interestingly, the Hill coefficient was 103 tl found to be 2.9, implying that some form of cooperative 104 binding is occurring, despite the expected 1:1 stoichiometry of 105 the Bim-Bcl-x_L pair. Nevertheless, control experiments where 106 STEPtag was replaced with bovine serum albumin, or where 107 gSTEP0 was replaced by cpGFP, confirmed that the 108 fluorescence response of the biosensor was dependent on 109 specific binding of the Bim peptide to the STEPtag 110 (Supplementary Figure S1b,c).

Having established that gSTEP0 could be used to detect the 112 presence of STEPtag *in vitro*, we next sought to improve the 113 properties of our sensor. We began by truncating the C- 114 terminus of gSTEP0 by removing the Thr-Arg linker (Figure 115 1d) as well as an additional 1 to 4 amino acids from cpGFP in 116 order to increase the size of the pore on the barrel surface, 117 which we hypothesized would improve $\Delta F/F_0$ by reducing 118 background fluorescence through increased quenching in the 119

Table 1. Properties of STEP Variants

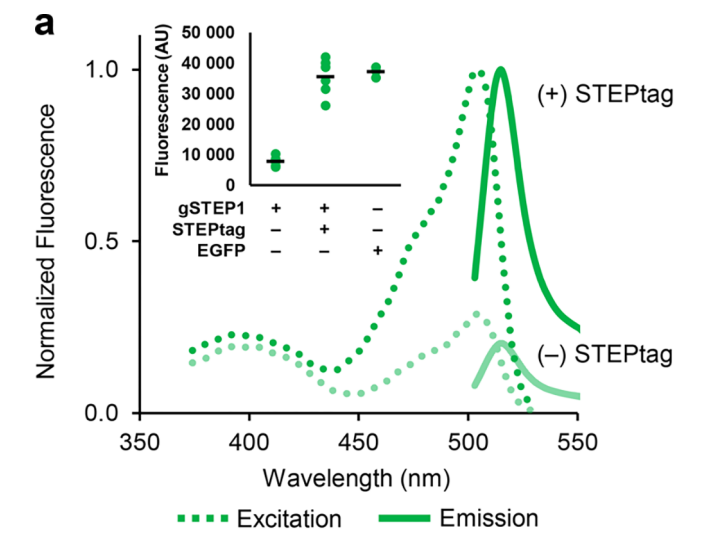
sensor	$\lambda_{\rm ex} ({\rm nm})^a$	$\lambda_{\rm em} (nm)^a$	$K_{\rm d}^{\ b}$ (nM)	in vitro $\Delta F/F_0^{\ b}$	in vivo $\Delta F/F_0^c$	$k_{\rm on} \ (\times 10^5 {\rm M}^{-1} \ {\rm s}^{-1})^d$	$k_{ m off}~({ m s}^{-1})^e$
gSTEP0	496 ± 1	513 ± 1	250 ± 40	1.4 ± 0.1	N.D. ^f	N.D. ^f	N.D. ^f
gSTEP1	504 ± 1	515 ± 1	120 ± 20	3.4 ± 0.4	11 ± 4	1.7 ± 0.2	0.020 ± 0.007

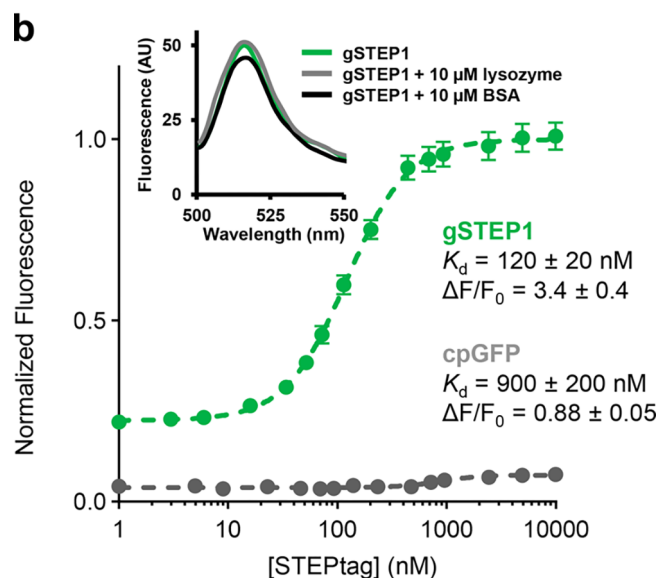
 $^an = 9$, mean \pm s.d. For comparison, excitation and emission wavelengths of EGFP are 488 and 507 nm, respectively. b Measured in solution using purified gSTEP (75 nM) and STEPtag (up to 10 μ M). For gSTEP0, n = 6, fit value \pm 95% confidence interval. For gSTEP1, n = 18, fit value \pm 95% confidence interval. c Calculated from the average fluorescence of individual cells expressing both gSTEP1 and STEPtag, or expressing only gSTEP1 (see Figure 3a). n = 2, mean \pm s.d. d Measured in solution using purified gSTEP1 (1 μ M) and STEPtag (5 μ M), n = 3, fit value \pm 95% confidence interval. d Calculated from the K_d and k_{on} . Error represents the propagated 95% confidence interval. d N.D. indicates not determined.

120 unbound state. The best truncated mutant, gSTEP0-T1, had 121 both the Thr-Arg linker and a single additional amino acid 122 from cpGFP removed (Supplementary Table S1), and we 123 found that it bound specifically to STEPtag with a $K_{\rm d}$ of 210 \pm 124 80 nM and a $\Delta F/F_0$ of 2.1 \pm 0.4 (Supplementary Figure S2, 125 Supplementary Table S2). Control experiments with this 126 improved variant confirmed that fusion of STEPtag using a 10-127 amino acid linker to either the N- or C-terminus of a protein of 128 interest does not substantially affect biosensor response or 129 binding affinity (Supplementary Figure S3).

Next, we replaced the mouse Bim peptide of gSTEP0-T1 131 with the human homologue or a range of synthetic variants 132 displaying tight binding to Bcl-x_L, 25 which we hypothesized 133 would enhance binding affinity to the STEPtag. Of these, the 134 human Bim peptide performed the best ($K_d = 170 \pm 40 \text{ nM}$, 135 $\Delta F/F_0 = 3.3 \pm 0.6$, Supplementary Table S2). In parallel, we 136 tested various linker lengths (1 to 5 amino acids) between the 137 original mouse Bim peptide and cpGFP in gSTEP0-T1 to 138 allow alternate binding poses of the STEPtag on the gSTEP 139 surface upon formation of the complex. We hypothesized that 140 changing the relative orientation of the binding partners could 141 enhance binding affinity or $\Delta F/F_0$ by allowing more favorable 142 noncovalent interactions between these molecules or causing a 143 larger change to the electrostatic environment of the 144 chromophore upon binding, respectively. We found that 145 addition of a four-amino acid linker (gSTEP0-T1-L4) 146 improved the binding affinity but not $\Delta F/F_0$ relative to 147 gSTEP0-T1 (Supplementary Table S2). Interestingly, replace-148 ment of the mouse Bim peptide in gSTEP0-T1-L4 by its 149 human homologue yielded a worse K_d and $\Delta F/F_0$ even though 150 human Bim performed better than mouse Bim in gSTEP0-T1. 151 Therefore, as a final step, we performed combinatorial 152 saturation mutagenesis of the four-amino acid linker 153 introduced between human Bim and cpGFP in gSTEP0-T1-154 L4, and screened the resulting library for improved brightness 155 and $\Delta F/F_0$ using fluorescence-activated cell sorting and 156 microplate-based binding assays, respectively (Methods). 157 This yielded our final improved variant, gSTEP1 (Figure 1d, 158 Table 1, Supplementary Table S1), which displays a $\Delta F/F_0$ of 159 3.4 \pm 0.4, equivalent to that of the original GCaMP ($\Delta F/F_0$ = 160 3.5), 16 and is as bright as the enhanced GFP (EGFP) from 161 Aequorea victoria²⁶ when fully bound to STEPtag (Figure 2a). 162 gSTEP1 binds specifically (Figure 2b) and rapidly (Figure 2c) 163 to STEPtag, with a $K_{\rm d}$ of 120 \pm 20 nM and a binding rate 164 constant ($k_{\text{on}} = 1.7 \pm 0.2 \times 10^5 \,\text{M}^{-1} \,\text{s}^{-1}$) that is comparable to 165 that of peptide antigen binding by antibodies.²

Next, we evaluated whether gSTEP1 could be used to detect 167 STEPtag expression in live E. coli cells, which we selected as a 168 case study given the fast GFP maturation rate in this 169 organism. To do so, we prepared an E. coli strain that 170 constitutively expresses a low basal concentration of gSTEP1 171 and in which STEPtag expression can be induced by the 172 addition of arabinose (Methods). In flow cytometry experi-173 ments, we observed that cells constitutively expressing gSTEP1 174 and overexpressing STEPtag were considerably brighter than 175 those that do not express the binding partner (Figure 3a), with 176 little overlap between the fluorescence distributions of the two 177 cell populations. Under these conditions, the mean fluo-178 rescence of the cellular population in the ON state was an 179 order of magnitude higher than that of the cellular population 180 in the OFF state, resulting in a $\Delta F/F_0$ of 11 \pm 4 (Table 1). 181 Taken together, these results demonstrate that the fluorescence 182 difference of gSTEP1 in the ON and OFF states is sufficient to





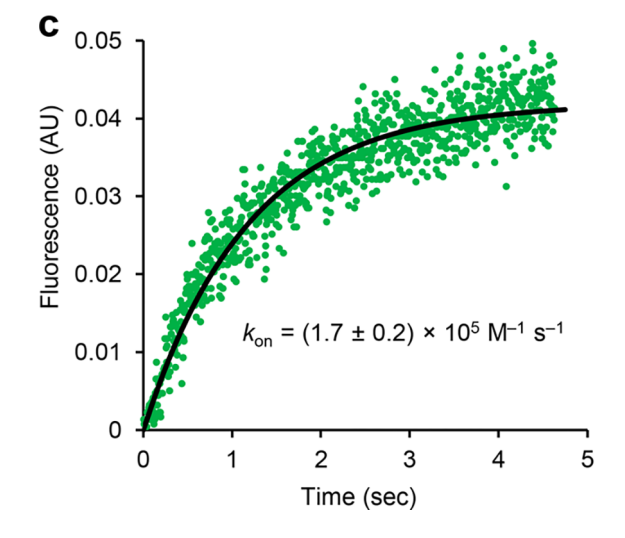


Figure 2. In vitro characterization of gSTEP1. All assays were performed in 20 mM sodium phosphate buffer containing 50 mM NaCl (pH 7.4). (a) Normalized excitation ($\lambda_{\rm em} = 550$ nm, dashed line) and emission ($\lambda_{\rm ex} = 485$ nm, full line) spectra of gSTEP1 (75 nM) in the presence or absence of saturating STEPtag (10 μ M). n = 3, average spectra shown. Inset: the fluorescence intensity at 515 nm ($\lambda_{\rm ex} = 485$ nm) of gSTEP1, in the presence or absence of saturating

Figure 2. continued

STEPtag, compared to 75 nM EGFP. n=6 for gSTEP1, n=3 for EGFP, mean values are shown as black lines. (b) Binding curves of 75 nM gSTEP1 (green) or cpGFP (gray) with STEPtag. Fluorescence is normalized to the maximum intensity observed for gSTEP1. Dashed lines represent fits of the Hill equation to the data (Hill coefficients of 1.5 or 2.2 for gSTEP1 or cpGFP, respectively). For the gSTEP1 binding curve, n=18, mean \pm SEM shown. For cpGFP, n=3, mean value shown. $K_{\rm d}$ and $\Delta F/F_0$ values were obtained from the fit and indicated with the 95% confidence interval around the fit values. Inset: emission spectra ($\lambda_{\rm ex}=485$ nm) of 75 nM gSTEP1 alone and in the presence of 10 μ M hen egg white lysozyme or bovine serum albumin (BSA). n=3, average spectra shown. (c) Rapid-mixing stopped-flow binding kinetics of a representative replicate of gSTEP1 mixed with saturating STEPtag. The black line represents a fit of the integrated rate equation to the data (Methods).

183 distinguish individual bacterial cells that express STEPtag from 184 those that do not.

Having demonstrated that gSTEP1 could be used to detect 186 the STEPtag in live E. coli cells at the steady-state, we evaluated 187 the ability of the biosensor to report on STEPtag concentration dynamics. To do so, we cultured the cells constitutively expressing gSTEP1 until they reached the 190 exponential growth phase, and then induced expression of 191 STEPtag by adding arabinose. We observed an immediate 192 fluorescence increase (Figure 3b), and the signal continued to 193 increase linearly for 20 min. Control experiments demon-194 strated that it was possible to modulate the rate of fluorescence 195 increase by reducing the amount of arabinose added, thereby 196 lowering the rate of STEPtag production (Supplementary 197 Figure S4). We also demonstrated that any metabolic load 198 from the presence of constitutively expressed gSTEP1 had a 199 minimal effect on arabinose-induced protein expression 200 (Supplementary Figure S5). To determine how long it takes 201 for protein expression to be detected by our biosensor, we 202 measured the baseline fluorescence of these cells prior to 203 induction of STEPtag expression, and used the noise in this 204 baseline data to set detection thresholds above the signal at 205 time of induction (t = 0 min). The standard deviation was used 206 to quantify the noise, such that the thresholds of 1, 2, and 3 207 standard deviations above the signal at t = 0 min represent 208 increasing levels of confidence that the increase in fluorescence 209 is due to the fluorescent reporter (Table 2). For cells 210 expressing both gSTEP1 and STEPtag, the threshold of 3 211 standard deviations of the baseline above the signal at 0 min 212 was reached in 1.6 \pm 0.2 min. By contrast, when we induced 213 expression of EGFP (maturation half-time = 25 min²⁶) using 214 the same promoter in cells containing only the EGFP 215 expression vector, it took 4 ± 1 min for it to reach the same 216 threshold, over twice as long as for gSTEP1. Of note, the rate 217 of fluorescence increase for EGFP accelerated with time, 218 reaching a steady state after approximately 10 min under these 219 conditions. Presence of this lag phase is consistent with slower 220 oxidation than folding/cyclization/dehydration during GFP 221 chromophore maturation. ²⁸ In the first 5 min following 222 induction of protein expression, gSTEP1 provided 6- to 10-223 fold higher fluorescence signal than EGFP, and this signal 224 remained higher for over 20 min (Figure 3). We also tested 225 Superfolder GFP (sfGFP), which folds and matures faster than 226 EGFP (maturation half-time = 13.6 min²⁹). Expression of 227 sfGFP using the same promoter also resulted in a lag phase, 228 albeit shorter than the one observed for EGFP (approximately

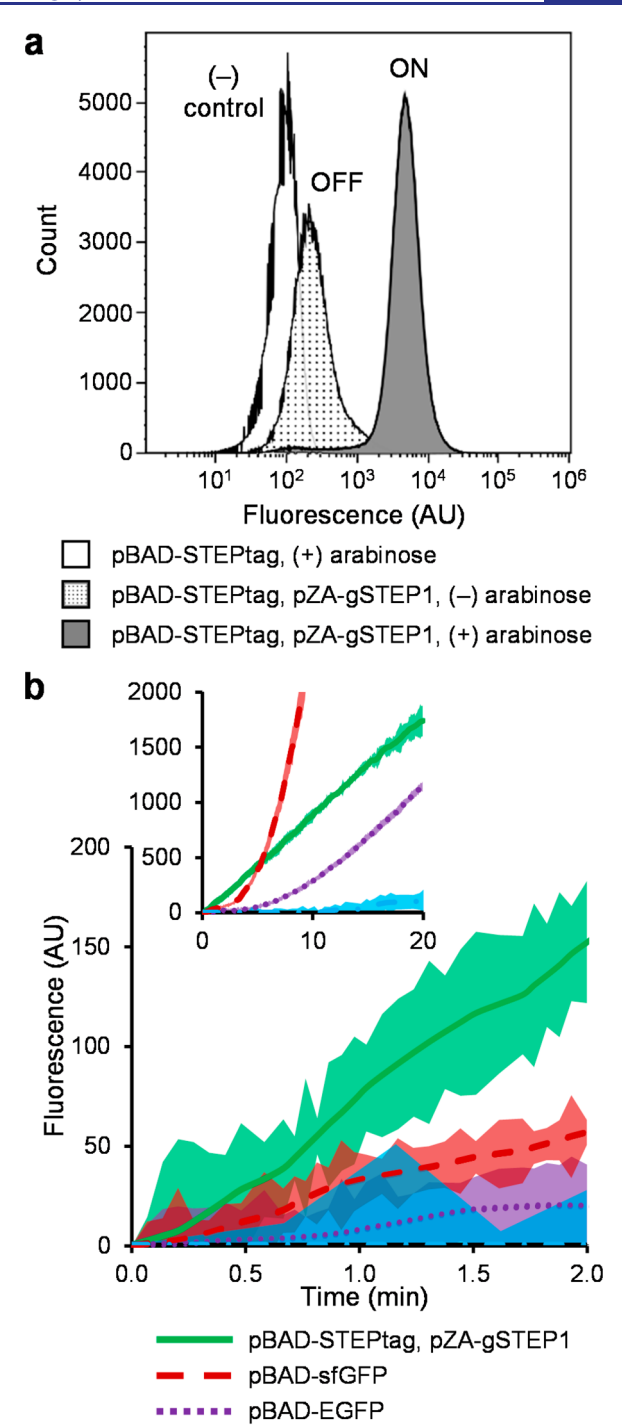


Figure 3. gSTEP1 enables rapid detection of protein expression in live bacterial cells. (a) Flow cytometry histograms of a representative biological replicate of gSTEP1 fluorescence in live *E. coli* cells expressing only STEPtag (negative control), gSTEP1 (OFF state), or both (ON state). The pZA vector constitutively expresses gSTEP1, while STEPtag expression from the pBAD vector is induced using 0.2% arabinose. (b) Time course of protein expression in live *E. coli*. Cells were grown to the end of the exponential growth phase (OD₆₀₀ = 1.1), then fluorescence was measured immediately after pBAD vectors containing either STEPtag (for cells constitutively expressing gSTEP1), EGFP, or sfGFP were induced with 0.45% arabinose. Each data set was blanked by the fluorescence signal at 0 min, and smoothed by three passes through a seven-point moving average filter. n = 4, the shaded area represents the mean \pm s.d. A negative control experiment is also shown, where cells constitutively expressing

pBAD-empty, pZA-gSTEP1

Figure 3. continued

gSTEP1 have an empty pBAD vector induced (pBAD-empty, pZA-gSTEP1). These cells were grown to OD_{600} of 0.6, and the shaded area represents the mean \pm s.d. for n=3. Inset: the same time course is shown, extended to 20 min to show the effects of longer-term induction. The same color scheme is used as in the main figure.

Table 2. Time Required to Reach a Specified Level of Fluorescence Following Induction of Protein Expression in Live *E. coli* Cells

		me to reach X standard deviations above initial fluorescence intensity $(min)^b$				
fluorescent reporter ^a	X = 1	X = 2	X = 3			
gSTEP1	0.63 ± 0.03	1.09 ± 0.06	1.6 ± 0.2			
EGFP	1.21 ± 0.09	3 ± 2	4 ± 1			
sfGFP	1.1 ± 0.4	2.1 ± 0.6	2.9 ± 0.4			

"gSTEP1 refers to cells expressing both gSTEP1 and STEPtag. EGFP and sfGFP refer to cells expressing only EGFP or sfGFP. STEPtag, EGFP, and sfGFP expression is under control of the araBAD promoter, and can be induced using arabinose. gSTEP1 is constitutively expressed. b Fluorescence of the bacterial cell population was measured for 10 min before induction of STEPtag, EGFP, or sfGFP expression using 0.45% arabinose, and this baseline signal was used to calculate the standard deviation serving as detection threshold $(n = 4, \text{mean} \pm \text{s.d.})$.

229 5 min to reach steady-state), and yielded a fluorescence 230 intensity increase of 3 standard deviations above the initial 231 signal in 2.9 ± 0.4 min (Table 2). These results demonstrate 232 that gSTEP1 enables faster detection of protein expression in 233 live *E. coli* cells than the use of traditional GFP reporters, which 234 should increase the temporal resolution of experiments aiming 235 to detect transiently expressed proteins or other fast biological 236 processes.

Compared with other genetically encoded fluorescent 237 238 biosensors used to track protein expression in real-time, 239 gSTEP1 has the benefits of not requiring the use of protein 240 translocation 11,12 or formation of large protein aggregates, 1 241 which should cause minimal perturbation to the subcellular 242 localization and physical properties of the protein of interest. 243 In the course of this work, a protein biosensor operating on a 244 similar principle to the STEP was published.³⁰ This sensor, 245 called Flashbody, is based on a cpGFP that is inserted between 246 heavy and light chain fragments from the variable region of an 247 antibody, which together bind specifically to a 7-amino acid 248 peptide tag fused to a protein of interest. Like gSTEP1, the 249 Flashbody has the benefits of not requiring translocation or 250 formation of large aggregates, and the response of the two 251 biosensors to their respective binding partner is similar ($\Delta F/F_0$ 252 \approx 3). However, gSTEP1 displays tighter binding (K_d of 120 253 nM for gSTEP1 vs 423 nM for the Flashbody), which could 254 allow detection of proteins present at lower concentrations 255 than the Flashbody limit of detection, and binds to its partner 256 with a rate constant 2 orders of magnitude higher than that of 257 the Flashbody ($k_{\rm on}$ of 1.7 × 10⁵ M⁻¹ s⁻¹ for gSTEP1 ν s 3.38 × 258 10³ M⁻¹ s⁻¹ for Flashbody). Taken together, these 259 advantages of gSTEP1 make it a useful alternative to other 260 biosensors for the rapid detection of protein expression in vivo 261 and in real time.

In conclusion, we have developed a genetically encoded fluorescent biosensor to rapidly detect protein expression within live bacterial cells. Because it is based on a circularly

permuted GFP, our sensor should be compatible with a wide 265 range of experimental setups. However, for some applications, 266 it may be necessary to further improve the biosensor's dynamic 267 range and sensitivity. This could be achieved by replacing the 268 Bim/STEPtag pair by alternate binding partners, and 269 optimizing the fluorescence response by random mutagenesis 270 followed by rounds of fluorescence-activated cell sorting using 271 the pZA-gSTEP1/pBAD-STEPtag strain developed here to 272 allow modulation of the STEPtag concentration. Alternate 273 colors should also be possible via the use of circularly 274 permuted yellow³¹ or red³² fluorescent proteins. We expect 275 that the engineering of a color palette of orthogonal STEP 276 biosensors will enable multiplexing for more complex imaging 277 experiments, opening the door to the in vivo visualization of 278 protein concentration dynamics in real time and at 279 unprecedented spatiotemporal resolution.

METHODS

Chemicals and Enzymes. All reagents used were of the 282 highest available purity. Synthetic oligonucleotides were 283 purchased from Eurofins MWG Operon. Restriction enzymes 284 and DNA-modifying enzymes were purchased from New 285 England Biolabs. All aqueous solutions were prepared using 286 water purified with a Barnstead Nanopure Diamond system. 287

Mutagenesis and Cloning. Codon-optimized (E. coli) 288 and his-tagged (N-terminus) sequences for gSTEP0 and 289 STEPtag (Supplementary Table S1) were purchased from 290 ATUM. Truncation mutants of gSTEP0 (T1-T4) were 291 obtained by polymerase chain reaction amplification of the 292 appropriate region of the gene, while mutants with added 293 linkers (L1-L5) or alternate Bim peptides (hBim, XXA1, 294 XXA4, G2gE, Y4eK) were generated using splicing by overlap 295 extension (SOE) mutagenesis (Supplementary Table S3).33 296 Briefly, for each mutagenesis step, two oligonucleotides 297 containing the desired mutations were ordered, one comple- 298 mentary to each strand of the template gene. Each of these 299 mutagenesis oligonucleotides was used in conjunction with a 300 flanking oligonucleotide, complementary to either the 5' or 3' 301 end of the template gene. Polymerase chain reaction 302 amplification of the template sequence using these two pairs 303 of oligonucleotides generated two DNA fragments that overlap 304 at the mutagenesis site. An equimolar mixture of these two 305 fragments was then further amplified using the two flanking 306 oligonucleotides, resulting in a complete gene sequence having 307 incorporated the mutations present in the mutagenesis 308 oligonucleotides. Amplification was performed using Vent 309 DNA Polymerase (New England Biolabs), following the 310 manufacturer's protocol. The combinatorial linker saturation 311 library was generated by SOE mutagenesis of gSTEP0-T1-L4 312 using oligonucleotides containing four consecutive NNS 313 degenerate codons, one for every position of the linker 314 sequence. All sequences were subcloned into pET11a vectors 315 (Novagen) via the NdeI/BamHI restriction sites. Gene 316 constructs for live-cell experiments (i.e., flow cytometry and 317 in vivo binding assays) were subcloned via NcoI/EcoRI or 318 HindIII/BamHI into either the pBAD/His A (Invitrogen) or 319 pZA23MCS (EXPRESSYS) vectors for inducible or con- 320 stitutive expression, respectively.

Aequorea victoria EGFP [Genbank AAB02572] was cloned 322 into pBAD/His A using XhoI/EcoRI, which added the pBAD 323 His tag/Xpress Epitope/EK site to the N-terminus. His-tagged 324 (C-terminus) Thermoascus aurantiacus xylanase 10A (TAX, 325 UniProtKB: P23360) in which the two catalytic residues were 326

327 mutated to alanine (E157A/E263A) cloned into a pET11a 328 vector via NdeI/BamHI was a gift from Stephen L. Mayo. 34 329 TAX-L10-STEPtag and STEPtag-L10-TAX constructs were 330 generated using SOE mutagenesis and cloned into pET11a 331 vectors as described above. His-tagged (N-terminus) sfGFP 332 cloned into a pBAD vector (pBAD-sfGFP) was a gift from 333 Michael Davidson and Geoffrey Waldo (Addgene plasmid 334 #54519; http://n2t.net/addgene:54519; RRID: Addg-335 ene_54519). All constructs were verified by sequencing the 336 entire open reading frame (see Supplementary Table S1 for 337 amino acid sequences), and transformed into either BL21-338 Gold(DE3) (Agilent) or TOP10 (Thermo Fisher) chemically 339 competent *E. coli* cells for pET11a, or pBAD and pZA vectors, 340 respectively.

Protein Expression and Purification. Transformed 342 *E. coli* cells harboring expression vectors were grown in 500 343 mL lysogeny broth (LB) supplemented with 100 μ g mL⁻¹ 344 ampicillin at 37 °C with shaking. When an OD₆₀₀ of 0.6–0.8 345 was reached, protein expression was induced by addition of 1 346 mM isopropyl β -D-1-thiogalactopyranoside (pET11a vectors) 347 or 0.2% arabinose (pBAD vectors). Following overnight 348 incubation at 16 °C with shaking, cells were harvested by 349 centrifugation and lysed with an EmulsiFlex-B15 cell disruptor 350 (Avestin). Following removal of cellular debris by centrifuga-351 tion, proteins were extracted and purified by immobilized

metal affinity chromatography using Profinity IMAC resin 352 (Bio-Rad) in a gravity flow column according to the 353 manufacturer's protocol. Eluted proteins were exchanged into 354 20 mM sodium phosphate buffer containing 50 mM NaCl (pH 355 7.4) and concentrated using Amicon Ultra-15 centrifugal filters 356 with a molecular weight cutoff of 3 kDa (Millipore) for 357 STEPtag, or Microsep Advance centrifugal filters with a 358 molecular weight cutoff of 10 kDa (Pall) for all other proteins. 359 Purified proteins were quantified by measuring absorbance at 360 280 nm in a 1 cm quartz cuvette with a SpectraMax Plus384 361 microplate spectrophotometer (Molecular Devices), and 362 applying Beer–Lambert's law using extinction coefficients 363 calculated with the ProtParam tool (https://web.expasy.org/ 364 protparam/).

In Vitro Binding Assays. All fluorescence measurements 366 were performed in Fluotrac 96-well plates (Greiner Bio-One) 367 on a Tecan Infinite M1000 plate reader using 75 nM of each 368 gSTEP variant in 20 mM sodium phosphate buffer containing 369 50 mM NaCl (pH 7.4). To calculate $K_{\rm d}$ and $\Delta F/F_0$ values, 370 gSTEP fluorescence intensity ($\lambda_{\rm ex}$ = 485 nm, $\lambda_{\rm em}$ = 515 nm) as 371 a function of STEPtag, TAX-L10-STEPtag, STEPtag-L10- 372 TAX, or control protein concentration (e.g., bovine serum 373 albumin [Bio-Rad] or an inactive mutant of Thermoascus 374 aurantiacus xylanase 10A purified as described above 34 was fit 375 to the Hill equation, accounting for ligand depletion: 35

$$\frac{[AB_{\text{eq}}]}{[A_0]} = \frac{(K_{\text{d}} + [A_0] + [B_0]) - \sqrt{(K_{\text{d}} + [A_0] + [B_0])^2 - 4[A_0][B_0]}}{2[A_0]}$$

378 where A (gSTEP variants) and B (STEPtag, TAX-L10-379 STEPtag, or STEPtag-L10-TAX) are the two binding proteins, 380 and $[A_0]$ and $[B_0]$ are the initial concentrations of each 381 protein. $[AB_{\rm eq}]$ is the equilibrium concentration of the bound 382 complex. For each experiment, a minimum of three replicates 383 were performed.

377

Fluorescence-Activated Cell Sorting. To improve the 385 signal-to-noise ratio in live cells, we aimed to isolate gSTEP0-386 T1-L4 variants that gave the brightest fluorescence from the 387 linker saturation library. To do so, we transformed the 388 gSTEP0-T1-L4 mutant library into E. cloni Elite electro-389 competent E. coli cells (Lucigen), which were plated on LB 390 agar supplemented with 100 μg mL⁻¹ ampicillin. Following 391 overnight incubation at 37 °C, a total of 10⁵ colonies from 392 multiple agar plates were collected, pooled together, and 393 cultured overnight in 10 mL LB supplemented with ampicillin. 394 Following extraction of plasmid DNA from this culture, the 395 library was transformed into BL21-Gold(DE3) electrocompe-396 tent E. coli cells, and plated on LB agar supplemented with 397 ampicillin. From these plates, 10⁵ colonies were collected, pooled together, and cultured overnight in 10 mL LB 399 supplemented with ampicillin. This bacterial culture was 400 diluted 100-fold into fresh LB supplemented with ampicillin 401 and grown to an OD₆₀₀ of 0.5-0.9. Because the leaky 402 expression of the T7 RNA polymerase in BL21-Gold(DE3) 403 provided sufficient quantities of protein to screen, the cells 404 were not further induced with isopropyl β -D-1-thiogalactopyr-405 anoside to limit their metabolic burden. After growth, cells 406 were centrifuged and pellets were washed twice with filter-407 sterilized 20 mM sodium phosphate buffer containing 50 mM 408 NaCl (pH 7.4). Resuspended cells were diluted in this buffer 409 to a concentration of approximately 5×10^7 colony forming units per mL. 36 The cells were then filtered twice using a 40- 410 μ m Falcon Cell Strainer (Fisher) to remove large particulates. 411 Fluorescence-activated cell sorting was performed on a MoFlo 412 AstriosEQ Cell Sorter (Beckman Coulter) using a 488 nm 413 laser for excitation and a 513/26 nm filter for detecting 414 fluorescence emission. Data analysis was performed with the 415 FlowJo software package (BD). This process was repeated 416 twice in succession, collecting 20 000 of the brightest cells each 417 time.

The collected cells were used to inoculate 50 mL of fresh LB 419 supplemented with ampicillin, and grown overnight at 37 °C 420 with shaking. This culture was used to streak an LB agar plate 421 supplemented with ampicillin. From this plate, 96 colonies 422 were picked into individual wells of a Nunc V96 MicroWell 423 polypropylene plate containing 200 µL of LB with 100 µg 424 mL⁻¹ ampicillin supplemented with 10% glycerol. The plate 425 was covered with a sterile gas permeable rayon film (VWR) 426 and incubated overnight at 37 °C with shaking. After 427 incubation, the mother plate was used to inoculate duplicate 428 Nunc V96 MicroWell polypropylene plates (daughter plates) 429 containing 250 μ L of LB with 100 μ g mL⁻¹ ampicillin per well. 430 Daughter plates were sealed with rayon film and incubated 431 overnight (37 °C, 250 rpm shaking). After incubation, the cells 432 were harvested by centrifugation and the pellets were washed 433 twice with phosphate buffered saline. These pellets were 434 resuspended and lysed in 100 μ L of Bugbuster protein 435 extraction reagent (Millipore) containing 5 U mL⁻¹ Benzonase 436 nuclease (Millipore) and 1 mg mL⁻¹ hen egg white lysozyme 437 (Omnipure). Following centrifugation to remove cellular 438 debris, the clarified lysate (30 μ L) was transferred to a 439 Fluotrac 96-well plate (Greiner Bio-One) for screening. To 440 each 30-µL lysate containing a different gSTEP0-T1-L4 441

442 variant, 150 µL of 20 mM sodium phosphate buffer containing 443 50 mM NaCl (pH 7.4) and 0 or 9 μM purified STEPtag was 444 added. Fluorescence was measured with a Tecan Infinite 445 M1000 plate reader. Emission spectra (λ_{ex} = 485 nm) were 446 measured from 500 to 560 nm. From these spectra, $\Delta F/F_0$ was 447 calculated for each protein variant, and the one with the best 448 response (gSTEP1) was analyzed further.

Rapid-Mixing Stopped-Flow Kinetics. Measurements 450 were performed using an RSM 1000 UV-vis rapid-scanning 451 spectrophotometer (Olis) equipped with a 1.24 mm-slit fixed 452 disk for single wavelength measurements, and plane gratings 453 with 400 lines mm⁻¹ and a 500 nm blaze wavelength. All other 454 fixed slits were set to 3.16 mm to maximize signal. Purified 455 gSTEP1 (1 μ M) and STEPtag (5 μ M) were loaded into the 456 spectrophotometer, which was kept at 37 °C using a 457 temperature control unit (Julabo). 300 μL of each sample 458 was pumped into the mixing chamber, and the fluorescence 459 was measured ($\lambda_{\rm ex}$ = 485 nm, $\lambda_{\rm em}$ = 515 nm). For each 460 combination of samples, the dead volume was cleared prior to 461 data collection. Control experiments were performed to 462 confirm that fluorescence increase was due to binding of 463 gSTEP1 to STEPtag (Supplementary Figure S6). The data was 464 fit to the integrated rate equation, accounting for ligand 465 depletion,³

$$[AB] = \frac{x \cdot y(e^{(x-y)k_{\text{on}}t} - 1)}{(xe^{(x-y)k_{\text{on}}t} - y)}$$

466 where A and B are the two binding proteins (gSTEP1 and 467 STEPtag), $x = [AB_{eq}], y = [A_0][B_0]/[AB_{eq}], \text{ and } t \text{ is the time.}$ 468 Three replicates were measured for this experiment, and the 469 data from all replicates were used for the fit.

Flow Cytometry. TOP10 E. coli cells (Invitrogen) 471 transformed with pZA-gSTEP1 and/or pBAD-STEPtag vectors 472 were cultured in 50 mL LB supplemented with 100 μ g mL⁻¹ 473 ampicillin (for cells containing pBAD) and/or 50 μg mL $^{-1}$ 474 kanamycin (for cells containing pZA). Cells were grown with 475 shaking at 37 °C to an OD₆₀₀ of 0.4-0.8, then the culture 476 containing both pBAD-STEPtag and pZA-gSTEP1 was split 477 equally into two flasks, one to be induced and the other to be 478 left uninduced. Following induction of cells containing pBAD 479 vectors with 0.2% arabinose, cultures were incubated for an $_{\rm 480}$ additional 60 min at 37 $^{\circ}\text{C}$ with shaking. Cells were then 481 harvested by centrifugation, and prepared for flow cytometry as 482 described in the cell sorting protocol above. Two biological 483 replicates of flow cytometry measurements were performed 484 using a Gallios flow cytometer (Beckman Coulter), set to 485 detect either 50 000 or 500 000 events per run. Fluorescence 486 was detected with a 525/40 filter ($\lambda_{\rm ex}$ = 488 nm), and data 487 analysis was performed using the Kaluza software package (Beckman Coulter). 488

In Vivo Binding Assays. TOP10 E. coli cells transformed 490 with the appropriate vectors were cultured as described for the 491 flow cytometry experiments above. Cells were grown with 492 shaking at 37 °C to an OD₆₀₀ of 0.6–1.1, after which 200 μ L of 493 each culture was transferred to a Fluotrac 96-well plate 494 (Greiner Bio-One). Fluorescence measurements were recorded 495 on an Infinite M1000 microplate reader equipped with an 496 injector module (Tecan), preheated to 37 °C (λ_{ex} = 488 nm, 497 $\lambda_{\rm em}$ = 514 nm). Measurements were taken every 2 min for 10 498 min, shaking the plate before each measurement, then protein 499 expression was induced by injecting 12 μ L of 8% arabinose 500 into the wells (final concentration of 0.45%), followed by 3 s of shaking and 2 s of settle time. Fluorescence was measured 501 every 2-6 s for an additional 20 or 40 min. For each 502 experiment, a minimum of three replicates were performed.

ASSOCIATED CONTENT

Supporting Information

The Supporting Information is available free of charge at 506 https://pubs.acs.org/doi/10.1021/acssynbio.0c00407.

Amino acid sequences, in vitro results for all constructs 508 tested, mutagenesis primer sequences, in vitro character- 509 ization of gSTEP0 and gSTEP-T1 with BSA controls for 510 specific binding, binding curves for STEPtag-TAX 511 fusions, time courses in live E. coli with varying arabinose 512 concentrations and plasmid controls (PDF)

504

505

514

517

518

519

520

521

522

523

524

525

531

532

534

535

537

538

546

AUTHOR INFORMATION

Corresponding Author

Roberto A. Chica – Department of Chemistry and Biomolecular 516 Sciences, University of Ottawa, Ottawa, Ontario K1N 6N5, Canada; orcid.org/0000-0003-3789-9841; Email: rchica@uottawa.ca

Authors

Matthew G. Eason – Department of Chemistry and Biomolecular Sciences, University of Ottawa, Ottawa, Ontario K1N 6N5, Canada

Antonia T. Pandelieva - Department of Chemistry and Biomolecular Sciences, University of Ottawa, Ottawa, Ontario K1N 6N5, Canada

Marc M. Mayer – Department of Chemistry and Biomolecular 527 Sciences, University of Ottawa, Ottawa, Ontario K1N 6N5, 528 Canada 529

Safwat T. Khan – Department of Chemistry and Biomolecular 530 Sciences, University of Ottawa, Ottawa, Ontario K1N 6N5, Canada

Hernan G. Garcia – Biophysics Graduate Group, Department of 533 Physics, Department of Molecular and Cell Biology, and Institute for Quantitative Biosciences-QB3, University of California, Berkeley, Berkeley, California 94720, United States 536

Complete contact information is available at: https://pubs.acs.org/10.1021/acssynbio.0c00407

Author Contributions

R.A.C. and H.G.G. conceived the project. M.G.E and S.T.K. 540 created the gene sequences. M.G.E. and A.T.P. engineered 541 proteins and characterized their properties. M.G.E. and 542 M.M.M. performed flow cytometry and in vivo binding assays. 543 All authors analyzed data. M.G.E. and R.A.C. wrote the 544 manuscript. H.G.G. edited the manuscript.

Notes

The authors declare no competing financial interest. 547 Plasmids containing STEPtag, STEPtag-L10-TAX, TAX-L10- 548 STEPtag, and gSTEP1 are available from Addgene (Plasmids 549 #159373-159376). 550

ACKNOWLEDGMENTS

R.A.C. acknowledges grants from the Canada Foundation for 552 Innovation (26503) and the Human Frontier Science Program 553 (RGP0041). H.G.G. was supported by the Burroughs 554 Wellcome Fund Career Award at the Scientific Interface, the 555 Sloan Research Foundation, the Human Frontiers Science 556 Program (RGP0041), the Searle Scholars Program, the Shurl 557

558 & Kay Curci Foundation, the Hellman Foundation, the NIH 559 Director's New Innovator Award (DP2 OD024541-01), and 560 an NSF CAREER Award (1652236). M.G.E. and M.M.M. are 561 the recipients of Ontario Graduate Scholarships and 562 postgraduate scholarships from the Natural Sciences and 563 Engineering Research Council of Canada. The authors thank 564 Shahrokh Ghobadloo for assistance with the fluorescence-565 activated cell sorting and flow cytometry experiments, Jeffrey 566 W. Keillor for use of the rapid-mixing stopped-flow 567 spectrophotometer, James A. Davey for providing the EGFP 568 gene, and Stephen L. Mayo for providing the Thermoascus 569 aurantiacus xylanase 10A expression vector.

570 **ABBREVIATIONS**

571 GFP, green fluorescent protein; STEP, sensor for transiently 572 expressed proteins; cpGFP, circularly permuted green 573 fluorescent protein; gSTEP, green fluorescent sensor for 574 transiently expressed proteins; EGFP, enhanced green 575 fluorescent protein; sfGFP, superfolder green fluorescent 576 protein; SOE, splicing by overlap extension; LB, lysogeny 577 broth.

578 REFERENCES

- 579 (1) Guet, C. C., Elowitz, M. B., Hsing, W., and Leibler, S. (2002) 580 Combinatorial synthesis of genetic networks. *Science* 296, 1466–1470. 581 (2) Nielsen, A. A. K., Der, B. S., Shin, J., Vaidyanathan, P., Paralanov, 582 V., Strychalski, E. A., Ross, D., Densmore, D., and Voigt, C. A. (2016) 583 Genetic circuit design automation. *Science* 352, aac7341.
- 584 (3) Matsumoto, Y., Ito, Y., Tsuru, S., Ying, B.-W., and Yomo, T. 585 (2011) Bacterial cells carrying synthetic dual-function operon 586 survived starvation. *J. Biomed. Biotechnol.* 2011, 489265.
- 587 (4) Tsien, R. Y. (1998) The green fluorescent protein. *Annu. Rev.* 588 *Biochem.* 67, 509-544.
- 589 (5) Balleza, E., Kim, J. M., and Cluzel, P. (2018) Systematic 590 characterization of maturation time of fluorescent proteins in living 591 cells. *Nat. Methods* 15, 47–51.
- 592 (6) Griffith, K. L., Shah, I. M., and Wolf, R. E., Jr (2004) Proteolytic 593 degradation of Escherichia coli transcription activators SoxS and 594 MarA as the mechanism for reversing the induction of the superoxide 595 (SoxRS) and multiple antibiotic resistance (Mar) regulons. *Mol.* 596 *Microbiol.* 51, 1801–1816.
- 597 (7) Tilly, K., Spence, J., and Georgopoulos, C. (1989) Modulation of 598 stability of the Escherichia coli heat shock regulatory factor sigma. *J.* 599 *Bacteriol.* 171, 1585–1589.
- 600 (8) Gedeon, T., and Bokes, P. (2012) Delayed protein synthesis 601 reduces the correlation between mRNA and protein fluctuations. 602 *Biophys. J.* 103, 377–385.
- 603 (9) Wang, X., Errede, B., and Elston, T. C. (2008) Mathematical 604 analysis and quantification of fluorescent proteins as transcriptional 605 reporters. *Biophys. J.* 94, 2017–2026.
- 606 (10) Berezhkovskii, A. M., and Shvartsman, S. Y. (2014) On the 607 GFP-based analysis of dynamic concentration profiles. *Biophys. J. 106*, 608 L13–15.
- 609 (11) Aymoz, D., Wosika, V., Durandau, E., and Pelet, S. (2016) 610 Real-time quantification of protein expression at the single-cell level 611 via dynamic protein synthesis translocation reporters. *Nat. Commun.* 612 7 11304
- 613 (12) Bothma, J. P., Norstad, M. R., Alamos, S., and Garcia, H. G. 614 (2018) LlamaTags: A Versatile Tool to Image Transcription Factor 615 Dynamics in Live Embryos. *Cell* 173, 1810–1822.
- 616 (13) Zhao, N., Kamijo, K., Fox, P. D., Oda, H., Morisaki, T., Sato, Y., 617 Kimura, H., and Stasevich, T. J. (2019) A genetically encoded probe 618 for imaging nascent and mature HA-tagged proteins in vivo. *Nat.* 619 *Commun.* 10, 2947.

- (14) Tanenbaum, M. E., Gilbert, L. A., Qi, L. S., Weissman, J. S., and 620 Vale, R. D. (2014) A protein-tagging system for signal amplification in 621 gene expression and fluorescence imaging. *Cell* 159, 635–646.
- (15) Boersma, S., Khuperkar, D., Verhagen, B. M. P., Sonneveld, S., 623 Grimm, J. B., Lavis, L. D., and Tanenbaum, M. E. (2019) Multi-Color 624 Single-Molecule Imaging Uncovers Extensive Heterogeneity in 625 mRNA Decoding. *Cell* 178, 458–472.
- (16) Nakai, J., Ohkura, M., and Imoto, K. (2001) A high signal-to-627 noise Ca(2+) probe composed of a single green fluorescent protein. 628 Nat. Biotechnol. 19, 137–141.
- (17) Tian, L., Hires, S. A., Mao, T., Huber, D., Chiappe, M. E., 630 Chalasani, S. H., Petreanu, L., Akerboom, J., McKinney, S. A., 631 Schreiter, E. R., Bargmann, C. I., Jayaraman, V., Svoboda, K., and 632 Looger, L. L. (2009) Imaging neural activity in worms, flies and mice 633 with improved GCaMP calcium indicators. *Nat. Methods* 6, 875–881. 634 (18) O'Connor, L., Strasser, A., O'Reilly, L. A., Hausmann, G., 635 Adams, J. M., Cory, S., and Huang, D. C. (1998) Bim: a novel 636 member of the Bcl-2 family that promotes apoptosis. *EMBO J.* 17, 637
- (19) Pang, X., Moussa, S. H., Targy, N. M., Bose, J. L., George, N. 639 M., Gries, C., Lopez, H., Zhang, L., Bayles, K. W., Young, R., and Luo, 640 X. (2011) Active Bax and Bak are functional holins. *Genes Dev.* 25, 641 2278–2290.
- (20) Muchmore, S. W., Sattler, M., Liang, H., Meadows, R. P., 643 Harlan, J. E., Yoon, H. S., Nettesheim, D., Chang, B. S., Thompson, C. 644 B., Wong, S. L., Ng, S. L., and Fesik, S. W. (1996) X-ray and NMR 645 structure of human Bcl-xL, an inhibitor of programmed cell death. 646 Nature 381, 335–341.
- (21) Oberstein, A., Jeffrey, P. D., and Shi, Y. (2007) Crystal 648 structure of the Bcl-XL-Beclin 1 peptide complex: Beclin 1 is a novel 649 BH3-only protein. *J. Biol. Chem.* 282, 13123–13132.
- (22) Kvansakul, M., Yang, H., Fairlie, W. D., Czabotar, P. E., Fischer, 651 S. F., Perugini, M. A., Huang, D. C., and Colman, P. M. (2008) 652 Vaccinia virus anti-apoptotic F1L is a novel Bcl-2-like domain-653 swapped dimer that binds a highly selective subset of BH3-containing 654 death ligands. *Cell Death Differ.* 15, 1564–1571.
- (23) Chen-Levy, Z., and Cleary, M. L. (1990) Membrane topology 656 of the Bcl-2 proto-oncogenic protein demonstrated in vitro. *J. Biol.* 657 *Chem.* 265, 4929–4933.
- (24) Nguyen, M., Millar, D. G., Yong, V. W., Korsmeyer, S. J., and 659 Shore, G. C. (1993) Targeting of Bcl-2 to the mitochondrial outer 660 membrane by a COOH-terminal signal anchor sequence. *J. Biol.* 661 *Chem.* 268, 25265–25268.
- (25) Dutta, S., Ryan, J., Chen, T. S., Kougentakis, C., Letai, A., and 663 Keating, A. E. (2015) Potent and specific peptide inhibitors of human 664 pro-survival protein Bcl-xL. *J. Mol. Biol.* 427, 1241–1253.
- (26) Cormack, B. P., Valdivia, R. H., and Falkow, S. (1996) FACS- 666 optimized mutants of the green fluorescent protein (GFP). *Gene 173*, 667 33–38.
- (27) Landry, J. P., Ke, Y., Yu, G. L., and Zhu, X. D. (2015) 669 Measuring affinity constants of 1450 monoclonal antibodies to 670 peptide targets with a microarray-based label-free assay platform. *J.* 671 *Immunol. Methods* 417, 86–96.
- (28) Reid, B. G., and Flynn, G. C. (1997) Chromophore Formation 673 in Green Fluorescent Protein. *Biochemistry* 36, 6786–6791.
- (29) Pedelacq, J. D., Cabantous, S., Tran, T., Terwilliger, T. C., and 675 Waldo, G. S. (2006) Engineering and characterization of a superfolder 676 green fluorescent protein. *Nat. Biotechnol.* 24, 79–88.
- (30) Wongso, D., Dong, J., Ueda, H., and Kitaguchi, T. (2017) 678 Flashbody: A Next Generation Fluobody with Fluorescence Intensity 679 Enhanced by Antigen Binding. *Anal. Chem.* 89, 6719–6725.
- (31) Baird, G. S., Zacharias, D. A., and Tsien, R. Y. (1999) Circular 681 permutation and receptor insertion within green fluorescent proteins. 682 *Proc. Natl. Acad. Sci. U. S. A.* 96, 11241–11246.
- (32) Carlson, H. J., Cotton, D. W., and Campbell, R. E. (2010) 684 Circularly permuted monomeric red fluorescent proteins with new 685 termini in the beta-sheet. *Protein Sci. 19*, 1490–1499.

- 687 (33) Horton, R. M., Ho, S. N., Pullen, J. K., Hunt, H. D., Cai, Z., and 688 Pease, L. R. (1993) Gene splicing by overlap extension. *Methods* 689 *Enzymol.* 217, 270–279.
- 690 (34) Privett, H. K., Kiss, G., Lee, T. M., Blomberg, R., Chica, R. A., 691 Thomas, L. M., Hilvert, D., Houk, K. N., and Mayo, S. L. (2012)
- 692 Iterative approach to computational enzyme design. Proc. Natl. Acad.
- 693 Sci. U. S. A. 109, 3790-3795.
- 694 (35) Hulme, E. C., and Trevethick, M. A. (2010) Ligand binding 695 assays at equilibrium: validation and interpretation. *Br. J. Pharmacol.*
- 696 161, 1219–1237.
- 697 (36) Myers, J. A., Curtis, B. S., and Curtis, W. R. (2013) Improving 698 accuracy of cell and chromophore concentration measurements using 699 optical density. *BMC Biophys.* 6, 4.
- 700 (37) Chen, Y., Song, X., Ye, S., Miao, L., Zhu, Y., Zhang, R. G., and 701 Ji, G. (2013) Structural insight into enhanced calcium indicator 702 GCaMP3 and GCaMPJ to promote further improvement. *Protein Cell* 703 4, 299–309.